Journal of ELECTRONIC MATERIALS, Vol. 48, No. 4, 2019
https://doi.org/10.1007/s11664-019-06948-7

TOPICAL COLLECTION: INTERNATIONAL CONFERENCE ON THERMOELECTRICS 2018

The Impact of Peltier Effect on the Temperature Field During Spark Plasma Sintering of Thermoelectric Materials

A.S. TUKMAKOVA,[1,2,3,4] K.L. SAMUSEVICH,[1] A.V. ASACH,[1] and A.V. NOVOTELNOVA[1]

1.—ITMO University, Lomonosova st. 9, aud. 3102, Saint-Petersburg, Russia 197101. 2.—e-mail: astukmakova@corp.ifmo.ru. 3.—e-mail: tukmashh@gmail.com. 4.—e-mail: tukmashh@rambler.ru

We report about the modelling of spark plasma sintering of a line of thermoelectric materials. A significant difference of sintering temperature ΔT_s from 15 K to 110 K was found in the samples studied. The Peltier effect on the graphite-thermoelectric interfaces results in such temperature difference. The rise of sintering temperature leads to the ΔT_s increase. ΔT_s in the vertical direction is 2–3 times higher than in the radial one. Electric insulation modelled in the horizontal graphite–thermoelectric interfaces reduced ΔT_s in all the types of numerically studied samples by 59–92%.

Key words: Thermoelectrics, SPS, spark plasma sintering, finite elements simulation, FEM

INTRODUCTION

Spark plasma sintering (SPS) technique is widely used for thermoelectric (TE) materials (thermoelectrics) fabrication. Ordinarily, it is implemented by pressure and pulsed direct current of an appliance to the sample consisting of a nano- or a micropowder.[1]

SPS allows the formation of new material with small grain size, high density and large area of the grain boundaries.[2,3] Pressure applied and sintering temperature T_s are the crucial technological parameters of SPS. They influence phase formation and stabilities, nanograin size, densification and final thermoelectric properties of the sample.

However, sintering temperature in a sample during SPS is difficult to measure. Ordinarily, such measurements are implemented using a pyrometer or a thermocouple. These approaches cannot provide precise measurements and the whole picture of a temperature field in a sample volume. The difference between temperature in the thermocouple aperture and a sample may reach tens of degrees.[4,5]

An automatic system of SPS apparatus adjusts current in accordance with data obtained from the thermocouple. In order to get precise data, simulation codes, calibration and other additional systems may be used.[5–7]

Moreover, the temperature field in a sample within SPS is inhomogeneous. Shijia et al. showed a difference of sintering temperature ΔT_s of 26°C between the center and the edge of zeolite sample at T_s = 1325 °C.[8] A ΔT_s of about 29°C in an alumina sample has been reported by Achenani et al.[9] The ΔT_s presence may be explained by the difference in thermal and electrical properties of a sample and setup elements, contact resistances, setup geometry, etc. The change of setup geometry and/or the conductivity of specific setup elements influence the heat transfer process and may decrease a temperature inhomogeneity.[9]

In the case of SPS of thermoelectrics a Peltier effect is added to the process picture. A pulsed direct current flows through the contacts between graphite and a thermoelectric sample (interfaces 1 and 2 in Fig. 1) that have rather high Seebeck coefficient values. ΔT_s of about 60°C has been obtained by numerical simulation and proved experimentally on the example of Mg_2Si and $MnSi_{1.4}$ thermoelectric samples by Maizza et al.[10]

(Received August 23, 2018; accepted January 8, 2019; published online January 18, 2019)

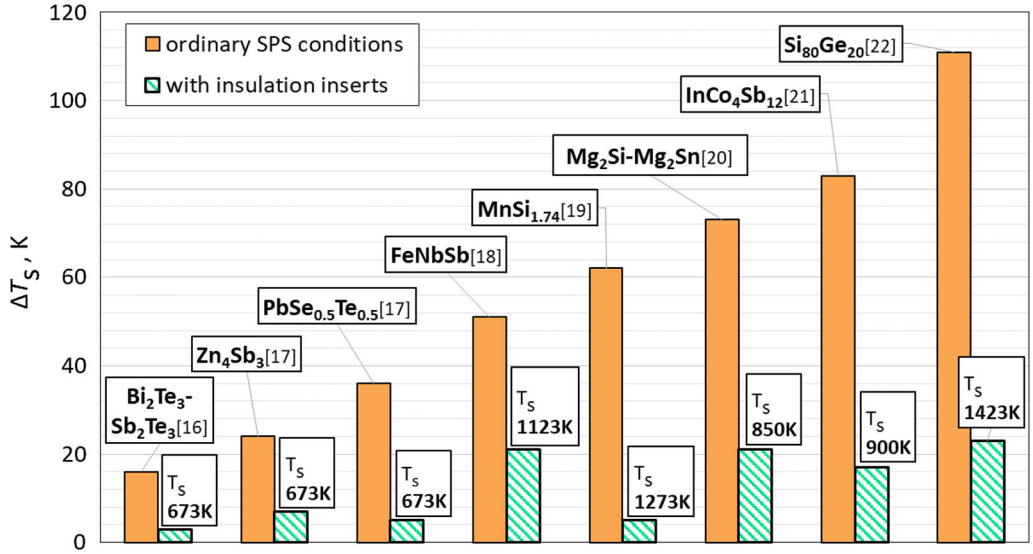

Fig. 1. The difference of sintering temperature during the SPS of different thermoelectrics and the reduced temperature difference in the case of SPS with insulating inserts.

The universal way of ΔT_s elimination in the context of thermoelectric materials sintering is not clear enough. In Ref. 11 an electrical insulation was placed between plungers and a La-filled skutterudite sample in order to eliminate Peltier effect manifestation. The authors reported a ΔT_s of less than 10 K in a sample with 200 mm diameter and 21 mm height that was supposed to has a large ΔT_s without insulation inserts.

A numerical approach, especially the finite element method (FEM), is a convenient way to analyze electrical, thermal and mechanical aspects of SPS.[4,6,12,13]

Since there are few works on SPS simulation taking into account a thermoelectric effect, a further investigation of this phenomenon seems to be an actual problem. In the current paper an FEM simulation was used to study the SPS process of low-, middle- and high-temperature thermoelectrics.

METHODS

The sintering process may be roughly separated into three main stages: (1) a powder treatment, (2) a consolidated compact dwell and (3) a slow cooling of the finite compact. In the model we considered only the first two stages. We did not take into account the third stage, as the main goal of the paper is a Peltier effect study and its most perceptible manifestation is expected to be within the maximum current occurring in the second stage. At the same time, the first stage cannot be excluded from the calculations as it has a direct impact on thermal and electrical processes during dwelling.

In order not to add a complexity to the model, no sample shrinkage was taken into consideration as it should not have a significant impact on Peltier effect. Initial sample size corresponded to the sintered sample.

No porosity or porosity change was considered in a direct way. However, an adjustment of sample physical properties was implemented in order to consider powder properties on the first SPS stage.

Setup geometry, current dependence on time, material properties of the setup elements and further model description can be seen from our previous work concerning SPS simulation using FEM.[14]

The modelling was implemented in Comsol Multiphysics software. The study was time-dependent. Normal current density was the time-dependent parameter. The model included two main physical interfaces: heat transfer in solids and electric currents. These interfaces were combined into the following multiphysical interfaces: (1) Joule heating and (2) thermoelectric effect. Mechanical processes description has not been added as it has no direct relation to the equations used.

The current density $\boldsymbol{j}$ and heat flux density $\boldsymbol{q}$ are related to their gradients in accordance with the following formula:

$$\boldsymbol{j} = -\sigma(\nabla\varphi + S\nabla \mathrm{T}), \tag{1}$$

$$\boldsymbol{q} = \kappa\nabla T + ST\boldsymbol{j} \tag{2}$$

where σ electric conductivity, φ electrochemical potential, S Seebeck coefficient, T absolute temperature, κ thermal conductivity.

The charge conservation law:

$$\mathrm{div} j = 0. \tag{3}$$

The energy balance:

$$c \cdot \rho \frac{\partial T}{\partial t} + \mathrm{div} \cdot \boldsymbol{q} + \boldsymbol{j} \nabla \varphi = 0, \tag{4}$$

where c is heat capacity, ρ is density, t is time.

To describe a convective heat exchange by means of water cooling on the upper and lower electrodes the following equation was used:

$$\boldsymbol{n} \cdot (\kappa \nabla T) = h \cdot (T_{\mathrm{ext}} - T_{\mathrm{e}}), \tag{5}$$

where $\boldsymbol{n}$ normal vector, h is a coefficient of heat transfer equal to 370 W/m^2 K, T_{ext} water temperature, T_{e} the electrode surface temperature.

Radiative heat removal from lateral sides of the setup elements:

$$\boldsymbol{n} \cdot (\kappa \nabla T) = \varepsilon\, \sigma_{\mathrm{SB}} \left(T_{\mathrm{amb}}^4 - T_0^4\right), \tag{6}$$

where $\sigma_{\mathrm{SB}} = 5.670 \times 10^{-8}$W/m K^{-4} is Stefan–Boltzmann constant; the factor ε equals 0.75 and 0.675 for graphite and steel, respectively[14]; the ambient temperature $T_{\mathrm{amb}} = 300$ K; T_0 lateral surface temperature.

All of the lateral setup surface was electrically insulated. Current density was applied to the upper steel electrode leading to Joule heating of setup elements and the sample. The current density was adjusted in order to obtain required T_{s} in a sample. The end of lower electrode had a zero potential.

Electrical and thermal contact resistances play a significant role in temperature and electrical fields formation.[13] However, horizontal resistance between graphite elements can be neglected during simulation.[15] On the high values of sintering pressure (more than 50 MPa) contacts can be neglected.[12] As sintering of thermoelectrics is usually implemented at a pressure of 50–100 MPa we did not include contact description into the model.

A line of different materials was used in the study. Thermoelectric properties of the materials were taken from Refs. 16–22 and are presented in Tables I, II and III. Electrical conductivity and Seebeck coefficient of graphite (Table IV) were measured using the differential and 4-probe methods at the NUST "MISiS", Moscow.

In order to consider powder properties within the first sintering stage we understate the values of electrical and thermal conductivity of the samples. During the first seconds of SPS these parameter values were close to zero and then increased with the temperature growth. At the beginning of the second stage they took the values corresponding to the consolidated sample (in accordance with the temperature).

Temperature dependence of Seebeck coefficient corresponded to the consolidated compacts on both sintering stages with no respect to the porosity. A heat capacity temperature dependence was admitted to be the same for all the materials of one composition.

RESULTS AND DISCUSSION

It is shown that sintering in an ordinary symmetric SPS setup configuration (die is symmetrically located, plungers have equal heights, no additional elements in the mold, etc.) cause gradient temperature field in thermoelectric samples.

Table I. Thermal conductivity of thermoelectric materials used in the simulation

	κ (W/m K)							
T (K)	Zn_4Sb_3	Bi_2Te_3-Sb_2Te_3	$PbSe_{0,5}Te_{0,5}$	Mg_2Si	FeNbSb	$InCo_4Sb_{12}$	Mg_2Si-Mg_2Sn	Si-Ge
300	0.75	1.2164	0.9695	1.6812	7.5992	1.8621	3.2349	2.6019
350	0.70	1.1213	0.9307	1.7355	7.1717	1.7586	3.1475	2.6151
400	0.72	1.0845	0.8906	1.7536	6.7308	1.6434	3.0710	2.6210
450	0.70	1.1074	0.8265	1.7536	6.3543	1.5503	3.0069	2.6324
500	0.70	1.1947	0.7904	1.7536	6.0258	1.4725	2.9192	2.6527
550	0.70	–	0.7772	1.7174	5.8154	1.3960	2.8339	2.6850
600	0.70	–	0.7937	1.7000	5.6759	1.3456	2.8464	2.7075
650	0.75	–	–	1.6812	6.7848	1.3083	2.8206	2.7172
700	–	–	–	1.5725	5.2542	1.2636	2.8227	2.7328
750	–	–	–	–	5.1121	1.2361	–	2.7537
800	–	–	–	–	5.8086	–	–	2.7682
850	–	–	–	–	4.9665	–	–	2.7784
900	–	–	–	–	4.8293	–	–	2.7883
950	–	–	–	–	4.7577	–	–	2.7980
1000	–	–	–	–	4.6860	–	–	2.8365
1050	–	–	–	–	4.6145	–	–	2.8991
1100	–	–	–	–	4.5455	–	–	2.9843
1150	–	–	–	–	–	–	–	3.0838

Table II. Electrical conductivity of thermoelectric materials used in the simulation

	σ (10^6 S/m)							
T (K)	Zn_4Sb_3	Bi_2Te_3-Sb_2Te_3	$PbSe_{0,5}Te_{0,5}$	$MnSi_{1.74}$	FeNbSb	$InCo_4Sb_{12}$	Mg_2Si-Mg_2Sn	Si-Ge
300	0.0408	0.1004	0.00008	0.0610	0.5961	0.0604	0.1487	0.0550
350	0.0392	0.0765	0.00027	0.0480	0.4980	0.0563	0.1364	0.0510
400	0.0370	0.0608	0.00064	0.0440	0.4000	0.0553	0.1247	0.0475
450	0.0364	0.0489	0.00127	0.0410	0.3600	0.0533	0.1147	0.0449
500	0.0357	0.0426	0.00202	0.0395	0.3200	0.0514	0.1066	0.0428
550	0.0351	–	0.00278	0.0360	0.2850	0.0500	0.0970	0.0410
600	0.0339	–	0.00348	0.0406	0.2500	0.0486	0.0866	0.0395
650	0.0328	–	0.00324	0.0324	0.2300	0.0480	0.0781	0.0381
700	–	–	0.00310	–	0.2100	0.0483	0.0722	0.0369
750	–	–	–	–	0.1900	0.0490	–	0.0359
800	–	–	–	–	0.1700	–	–	0.0348
850	–	–	–	–	0.1550	–	–	0.0336
900	–	–	–	–	0.1400	–	–	0.0325
950	–	–	–	–	0.1250	–	–	0.0314
1000	–	–	–	–	0.1100	–	–	0.0300
1050	–	–	–	–	–	–	–	0.0285
1100	–	–	–	–	–	–	–	0.0276
1150	–	–	–	–	–	–	–	0.0271

Table III. Seebeck coefficient of thermoelectric materials used in the simulation

	S (μV/K)							
T (K)	Zn_4Sb_3	Bi_2Te_3-Sb_2Te_3	$PbSe_{0,5}Te_{0,5}$	Mg_2Si	FeNbSb	$InCo_4Sb_{12}$	Mg_2Si-Mg_2Sn	Si-Ge
300	132	197	– 218	108	70	– 195	– 142	125
350	155	219	– 255	120	81	– 208	– 160	138
400	162	225	– 285	142	92	– 221	– 176	151
450	175	223	– 302	168	101	– 231	– 189	163
500	180	205	– 314	180	110	– 239	– 202	173
550	190	–	– 318	194	121	– 245	– 213	182
600	198	–	– 314	200	130	– 246	– 225	194
650	208	–	– 303	207	140	– 243	– 231	206
700	212	–	–	211	148	– 237	– 234	216
750	–	–	–	–	159	– 227	–	225
800	–	–	–	–	166	–	–	233
850	–	–	–	–	175	–	–	242
900	–	–	–	–	182	–	–	249
950	–	–	–	–	186	–	–	256
1000	–	–	–	–	192	–	–	261
1050	–	–	–	–	196	–	–	265
1100	–	–	–	–	198	–	–	267
1150	–	–	–	–	–	–	–	266

Table IV. The properties of the graphite used in the simulation

T (K)	κ (W/m K)	σ (S/m)	c_p (J/kg K)	S (μV/K)
300	91.3	113,974	800	6.96
400	90.2	108,405	995	6.96
500	84.6	101,192	1208	4.66
600	78	93,971	1381	1.34
700	71.7	89,120	1518	– 2.04
800	65.9	85,605	1629	– 4.70
900	60.9	78,893	1718	– 6.07

Temperature gradients in both radial and vertical directions exist.

In Fig. 1 the difference of sintering temperature ΔT_s in the samples volume is presented. ΔT_s was calculated as the difference between minimum and maximum T_s values in the sample volume. The results obtained for silicide samples are close to the experimental results for the samples with rather close properties.[10] This may be considered as a proof of the presented model adequacy. In our case ΔT_s is a bit higher. This may be due to the difference in composition and sample size.

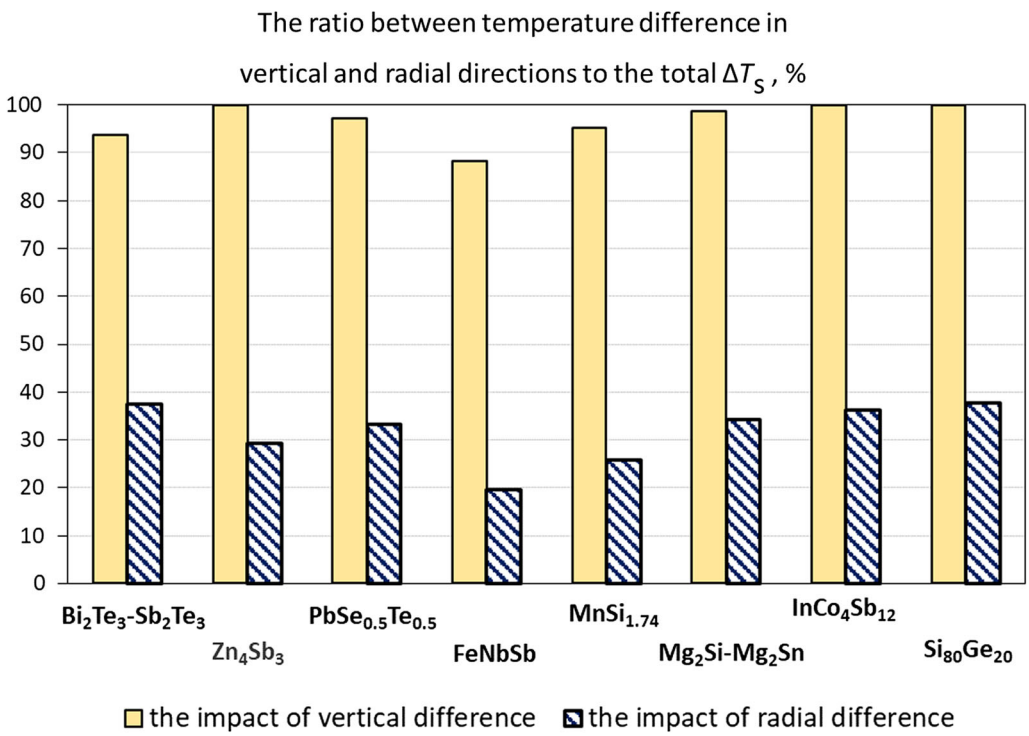

Fig. 2. The ratio between temperature difference in radial and vertical directions to the total difference of sintering temperature in a sample volume.

In general, the increase of sintering temperature leads to the ΔT_s increase. The lowest ΔT_s was found in bismuth and antimony telluride solid solutions (16 K) and the highest in the silicon germanium alloy (111 K). However, it is not a strict tendency. For example, magnesium silicide based solid solutions and cobalt antimonite based scutterudites showed a ΔT_s of 72° and 83°, respectively, at sintering temperatures of 850–900 K. At the same time, high manganese silicide and half-Heusler showed lower ΔT_s of 62° and 51° at higher sintering temperatures of 1273 K and 1123 K, respectively.

It seems that the temperature difference in the TE sample during SPS depends mostly on Peltier effect manifestation between graphite plungers and the sample.

For example, the sintering temperature difference in Mg_2Si-Mg_2Sn samples do not exceed 10 K if no TE effect is included into the model description (versus 62 K for model with thermoelectric effect). For Ge-Si sample ΔT_s value is 22 K if no TE effect is considered (versus 111° for a model with thermoelectric effect).

It can be seen in Fig. 2 that the ratio between vertical temperature difference and total ΔT_s has values from 88% to 100%. At the same time, this ratio for the radial ΔT_s is 20% to 38%. No increase of radial temperature difference impact to the total ΔT_s was found within the rise of sintering temperature.

In order to decrease Peltier heat release, electrical insulation may be used. Insulating inserts (mica foil, for example) can be placed between the sample and the plungers as it was proposed in.[11] We simulated the SPS process with such insulation; the results are shown in Fig. 1. The most effective reduction of ΔT_s was found in $MnSi_{1.74}$ sample; ΔT_s was reduced by 92%. This method was less effective for FeNbSb, but still the temperature difference was reduced by 59%.

Hence, electrical insulation allows suppressing the Peltier effect. This approach is mostly effective for vertical temperature gradient elimination, which is higher than the radial one.

CONCLUSION

It was reported earlier mostly on the example of metallic and ceramic samples that ΔT_s rises with the increase of T_s. The results of current work show the same tendency for thermoelectrics sintering.

The higher temperature gradient values was found in the samples with higher sintering temperature. Vertical temperature difference significantly higher than radial one for the samples of different composition.

An insert of electrical insulation placed in the interfaces between the plungers and a sample helps to significantly reduce ΔT_s. However, such approach prevents the current pass through the sample volume. That may lead to the suppression of the effects specific for SPS and have an impact on the structure and phase composition. More studies are needed to investigate this phenomenon.

ACKNOWLEDGMENTS

The reported study was funded by RFBR according to the research Project No. 18-38-00371.

REFERENCES

1. O. Guillon, J. Gonzalez-Julian, B. Dargatz, T. Kessel, G. Schierning, J. Räthel, and M. Herrmann, *Adv. Eng. Mater.* 16, 7 (2014).
2. Z.A. Munir, U. Anselmi-tamburini, and M. Ohyanagi, *J. Mater. Sci.* 41, 763 (2006).
3. R. Chaim, M. Levin, A. Shlayer, and C. Estournes, *Adv. Appl. Ceram.* 107, 159 (2008).
4. G. Molenat, L. Durand, J. Galy, and A. Couret, *J. Metall.* 2010, 9 (2010).
5. A. Zavaliangos, J. Zhang, M. Krammer, and J.R. Groza, *Mater. Sci. Eng. A* 379, 218 (2004).
6. S. Munoz and U. Anselmi-Tamburini, *J. Mater. Sci.* 45, 6528 (2010).
7. A. Pavia, L. Durand, F. Ajustron, V. Bley, G. Chevallier, A. Peigney, and C. Estournès, *J. Mater. Process. Technol.* 213, 1327 (2013).
8. G. Shijia, X. Zhang, L. Wang, X. Gan, Z. Shen, and W. Jiang, *J. Eur. Ceram. Soc.* 35, 1599 (2015).
9. Y. Achenani, M. Saâdaoui, A. Cheddadi, and G. Fantozzi, *Mater. Des.* 116, 504 (2017).
10. G. Maizza, G.D. Mastrorillo, S. Grasso, H. Ning, and M.J. Reece, *J. Mater. Sci.* 52, 10341 (2017).
11. T. Tomida, A. Sumiyoshi, G. Nie, T. Ochi, S. Suzuki, M. Kikuchi, K. Mukaiyama, and J.Q. Guo, *J. Electron. Mater.* 46, 2944 (2017).
12. U. Anselmi-Tamburini, S. Gennari, J.E. Garay, and Z.A. Munir, *Mater. Sci. Eng. A* 394, 139 (2005).
13. C. Manière, A. Pavia, L. Durand, G. Chevallier, K. Afanga, and C. Estournès, *J. Eur. Ceram. Soc.* 36, 741 (2016).
14. L.P. Bulat, A.V. Novotelnova, A.S. Tukmakova, D. Yerezhep, V.B. Osvenskii, A.I. Sorokin, V.P. Panchenko, L.V. Bochkov, and S. Asmontas, *J. Electron. Mater.* 47, 1589 (2018).
15. A. Cincotti, A.M. Locci, R. Orru, and G. Cao, *AIChE J.* 53, 703 (2007).
16. B. Madavali, H.-S. Kim, C.-H. Lee, D.-S. Kim, and S.-J. Hong, *J. Electron. Mater.* (2018). https://doi.org/10.1007/s11664-018-6706-7.
17. S. Li, J. Pei, D. Liu, L. Bao, J.-F. Li, H. Wu, and L. Li, *Energy* 113, 35 (2016).
18. C. Fu, T. Zhu, Y. Liu, H. Xiea, and X. Zhao, *Energy Environ. Sci.* 8, 216 (2015).
19. Y. Sadia, L. Dinnerman, and Y. Gelbstein, *J. Electron. Mater.* 42, 7 (2013).
20. M.I. Fedorov, V.K. Zaitsev, and G.N. Isachenko, *Solid State Phenom.* 170, 286 (2011).
21. V.V. Khovaylo, T.A. Korolkov, A.I. Voronin, M.V. Gorshenkov, and A.T. Burkov, *J. Mater. Chem. A.* 5, 3541 (2017).
22. A. Usenko, D. Moskovskikh, M. Gorshenkov, A. Voronin, A. Stepashkin, S. Kaloshkin, D. Arkhipov, and V. Khovaylo, *Scr. Mater.* 127, 63 (2017).